Nanoindentation study of hydride diffusion layer in commercial pure titanium

Qian Wang, Jean-Sébastien Lecomte, Christophe Schuman, Laurent Peltier

Nanoindentation study of hydride diffusion layer in commercial pure titanium

Qian Wang, Jean-Sébastien Lecomte, Christophe Schuman, Laurent Peltier

Nanoindentation study of hydride diffusion layer in commercial pure titanium

Qian Wang [a,b,**], Jean-Sébastien Lecomte [a,b,***], Christophe Schuman [a,b,*], Laurent Peltier [a,b]

[a] Laboratoire D'Etude des Microstructures et de Mécanique des Matériaux (LEM3), Université de Lorraine, CNRS, Arts et Métiers ParisTech, Metz, 57073, France
[b] Laboratory of Excellence on Design of Alloy Metals for Low-mAss Structures (DAMAS), Université de Lorraine, Metz, 57073, France

A B S T R A C T

In this work, the mechanical properties of hydride diffusion layer were thoroughly researched by nanoindentation technique. For the first time, the clear section microstructure of hydride diffusion layer was revealed under scanning electron microscope with complicated interactions of hydride plates near the interface between hydride layer and titanium matrix. The hydride layer section has higher hardness and lower modulus towards titanium matrix due to the hard nature and easier crack nucleation of hydride precipitation. Besides, the hardness of titanium matrix shows considerable anisotropy. The anisotropic hardness of sample surface was studied before and after hydrogen charging. The hardness of titanium matrix decreases with the increase of deviation angle between ***c***-axis and surface normal. The hydride layer formed in the titanium grain with more favorable orientation for hydride transformation tends to possess higher indentation hardness.

1. Introduction

Environment sensitive failure, particularly the hydrogen assisted mechanical degradation or hydrogen embrittlement, is a longstanding problem in material science, which occurs more easily with the increase of hydride precipitation. Hydrogen embrittlement in titanium occurs by hydrogen absorption near the crack tip and the precipitation of brittle hydride, thus promoting crack formation in a stress corrosion cracking process [1,2]. Three types of hydride phases have been found depending on the hydrogen concentration: face-centered tetragonal (FCT) TiH, face-centered cubic (FCC) TiHx (with x ranging between 1.5 and 2) and FCT TiH_2 [3–7]. In addition, four orientation relationships (ORs) are determined between hexagonal close packed (HCP) Ti matrix and FCT/FCC hydride [3–6] (see Table 1).

The hard nature of hydride and the strain incompatibility between hydride and matrix material are the reasons for the hydride enhanced hardening process [8]. Therefore, it is important to understand the mechanical properties of the hydride for the prevention of mechanical degradation. Nanoindentation test is a good method to measure the nanomechanical properties of hydride. According to the previous studies [9,10], the hydride diffusion layer formed by electrolytic hydrogen charging has higher nanohardness and lower elastic modulus than titanium matrix. Conforto et al. [11,12] also studied the mechanical characteristics of epitaxial hydride layer, plastic deformation were demonstrated in indentation tests up to more than 1% strain. The micro-crack or void nucleation can be formed by the internal stress concentration resulting from the interaction between hydride and plastic deformation modes.

In addition, the microstructure and some mechanical behaviors of hydride precipitation are related to the parent grain orientation. Wang et al. [13,14] proposed that the microstructure of hydride precipitation and hydride-induced plastic deformation are strongly dependent on the orientation of titanium matrix. Hydride-induced hardening in pure Zr is also dependent on the crystal orientation and relationship between slip plane and hydride habit plane, which is more significant when the slip plane close to the hydride habit plane [15]. Furthermore, the HCP

* Corresponding author. Laboratoire D'Etude des Microstructures et de Mécanique des Matériaux (LEM3), Université de Lorraine, CNRS, Arts et Métiers ParisTech, Metz, 57073, France.
** Corresponding author. Laboratoire D'Etude des Microstructures et de Mécanique des Matériaux (LEM3), Université de Lorraine, CNRS, Arts et Métiers ParisTech, Metz, 57073, France.
*** Corresponding author. Laboratoire D'Etude des Microstructures et de Mécanique des Matériaux (LEM3), Université de Lorraine, CNRS, Arts et Métiers ParisTech, Metz, 57073, France.
E-mail addresses: qian.wang@univ-lorraine.fr (Q. Wang), jean-sebastien.lecomte@univ-lorraine.fr (J.-S. Lecomte), christophe.schuman@univ-lorraine.fr (C. Schuman).

Table 1

Four orientation relationships of hydride transition.

	Orientation relationship	Interface plane
OR1	$\{0001\}//\{001\}, <1\bar{2}10>//<110>$	$\{10\bar{1}0\}//\{1\bar{1}0\}$
OR2	$\{0001\}//\{1\bar{1}1\}$ (angle of 4°), $<1\bar{2}10>//<110>$	$\{10\bar{1}3\}//\{1\bar{1}0\}$
OR3	$\{10\bar{1}0\}//\{1\bar{1}1\}, <1\bar{2}10>//<110>$	$\{0001\}//\{1\bar{1}2\}$
OR4	$\{\bar{1}011\}//\{001\}, <1\bar{2}10>//<110>$	$\{10\bar{1}1\}//\{1\bar{1}\bar{1}\}$

titanium shows strong anisotropy due to fewer slip systems. The anisotropic hardness of titanium was studied by Fizanne-Michel et al. [16] and Fitzner et al. [17]. The indentation hardness values decrease as the stress axis deviates from the [0001] direction. Therefore, it can be reasonably speculated that the indentation hardness of hydride layer are also influenced by the parent titanium orientation. To study this, titanium grains with random orientations were followed before and after hydrogen charging to investigate the relationship between the hardness of hydride layer and parent titanium orientation.

In the present paper, the mechanical properties of titanium hydride formed by electrolytic hydrogen charging were studied by means of nanoindentation technique. At first, the hardness and modulus of hydride layer section is measured and analyzed. Next, the anisotropic hardness of the titanium matrix and hydride precipitation is determined. The reason for the orientation dependent hardness of hydride and titanium matrix is analyzed.

2. Experimental methods

In the current work, the material used was rolled commercially pure titanium T40 (ASTM grade 2) sheet with the thickness of 1.5 mm and annealed at 800 °C for 3 h under high vacuum condition. The obtained material was fully recrystallized with an average grain size of ~50 μm. Due to limited sample thickness (1.5 mm), transverse direction (***TD***) and rolling direction (***RD***) surfaces were not sufficient to do analysis and not available for the nanoindentation test. Thus, for the investigation on the section of hydride layer (Sample A), ***TD*** surface was taken as diffusion surface and normal direction (***ND***) surface as observation surface of hydride layer section. The ***ND*** surface of Sample B was hydrogen diffusion surface. 44 grains with different orientations were measured by nanoindentation test before and after hydrogen charging to study the mechanical property change. According to our previous work [13], the texture of diffusion surface plays an important role on the hydride transformation. ***ND*** and ***RD*** surfaces are favorable for OR2 and OR1 hydride transformation, respectively. In this work, ***TD*** surface in Sample A had better orientation distribution covering both OR1 and OR2 favorable grains. As for Sample B, the selected grains had random orientations. Therefore, the texture of sample surfaces cannot significantly affect the results.

The details of the sample preparation are present here. The ***TD*** surface of initial Sample A was ground with 500–2000 grit SiC and then rough polished with 9–3 μm diamond, followed by 20 s electrolytic polishing to obtain free-stress surface. Electrolytic polishing was performed with a solution of 5% perchloric acid, 35% butan-*l*-ol and 60% of methanol at 40 V at temperatures lower than 5 °C [18]. After hydrogen charging, the sample were mounted with Struers Polyfast resin to protect the diffusion surface during the metallographic preparation process. The mounted sample was ground until 3 μm diamond and attack polished 20 min with the solution of 50 mL MASTERMET 2 colloidal silica, 10 mL H_2O_2 (30%) and 5 mL Kroll's reagent [19]. The attack polishing can reveal the interface microstructure between hydride layer and titanium matrix and is more moderate than argon ion polishing in Ref. [14]. For Sample B, the initial microstructure for Electron Backscatter Diffraction (EBSD) characterization was obtained by the same method with Sample A. To follow the same area including selected 44 grains before and after hydrogen charging, the zone of interest at the center of sample was marked by four micro-indentations. To prevent the influence of the corrosion of hydrogen charging solution on the hardness of diffusion surface, the hydrogenated surface was slightly electrolytic polished for 5 s before nanoindentation test.

Hydrogen was introduced into sample surface by an electrolytic method in an electrolyte consisting of 1/3 vol phosphoric acid and 2/3 vol glycerin under an applied current density of 2 kA/m^2 for 168 h. The schematic of the hydrogen charging system was presented in Fig. 1a. Enough hydride diffusion layer can be formed after 168 h charging. The hydrogen concentration of the sample with hydride layer is around 123 wt ppm, which was measured by thermal desorption analysis, the same as that in Ref. [13], at the Welding and Joining Institute (ISF) of the RWTH Aachen University. The characterization was performed using Zeiss Supra-40 and JSM 6490 scanning electron microscope (SEM) equipped with an EBSD camera. According to the X-ray diffraction result in Ref. [20], FCC hydride is dominant hydride phase after 168 h hydrogen charging. Moreover, it is difficult to accurately distinguish FCC and FCT hydride phases by EBSD, only FCC hydride was chosen as indexed phase in this work.

Nanoindentation tests were conducted using the nanoindenter NHT_2 from Anton Paar equipped with a continuous stiffness measurements modulus and Berkovich tip indenter (142.3°). The indentation hardness (H_{IT}) and plane strain modulus (E*) were extracted from the unloading part of load-depth curves by using Oliver and Pharr model [21]. For Sample A, the indentation arrangement to measure the hydrogenated sample section follows the method of [9], as shown in Fig. 1b. 35 indents were arranged along the tilted red line started from resin to titanium regions with respective 5 μm and 1 μm separation along ***x*** and ***y*** axes. An adjusting the depth offset (ADO) procedure was performed after each three indentations to prevent the unpredictable surface topography variation. The average H_{IT} and E* values related to the distance from the diffusion surface around 1–30 μm are calculated from five indentation lines. To measure the anisotropic mechanical properties of Sample B, 6 indentations plus 1 ADO were pressed in the equivalent 44 grains before and after hydrogenation charging. The indentations after hydrogen charging were performed far from the indents before charging to prevent the influence of each other. The influence of the grain boundaries was minimized by choosing indents in the grain interior more than 2 μm from grain boundaries [22]. The average hardness of each grain was calculated and analyzed together with crystal orientation. The inverse pole figure (IPF) related to the nanohardness was drawn with the hardness IPF file of a free Python library developed by Jean-Sébastien Lecomte (https://github.com/pyOriLib).

3. Results and discussion

3.1. Section of hydride diffusion layer

3.1.1. Section microstructure

The section microstructure of hydrogenated sample is shown in the SEM image (see Fig. 2a). The hydride layer can be found between the resin and titanium matrix, which reveals the non-uniform hydride formation during the hydrogen charging at room temperature. Indeed, during hydrogen diffusion in titanium, lath-shaped hydride forms randomly at the early stage, then forms colonies and eventually a layer [24]. The microstructure of the area inside the green box is characterized under EBSD measurement, as shown in Fig. 2b and c. Phase map is presented in Fig. 2b, in which the hydride and titanium phases are colored by respective green and red. The green layer corresponds to the dark gray hydride layer in the SEM image. In addition, inside the titanium matrix, there also appear some hydride particles. Thus, it can be derived that hydride particles can be formed first before the hydride plate and hydride layer during hydrogen diffusion. The grain boundaries (black lines) inside diffusion layer show the complicated hydride interactions, which can be observed more clearly in Fig. 2c. The IPF map is projected by ***TD*** parallel to hydrogen diffusion direction.

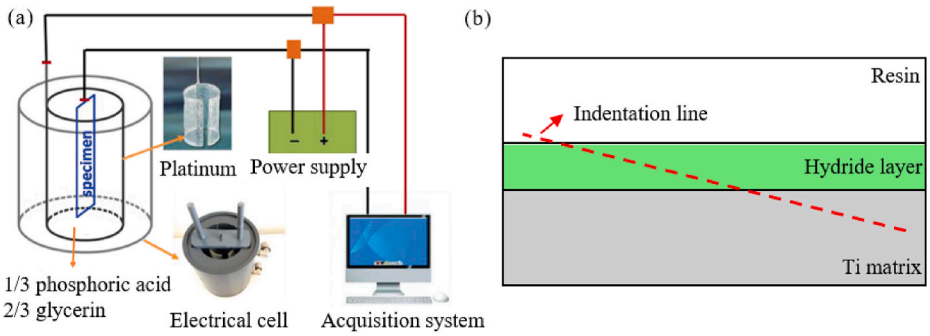

Fig. 1. (a) Schematic presentation of the hydrogen charging system [23]. (b) Schematic of hydride diffusion layer and indentation arrangement.

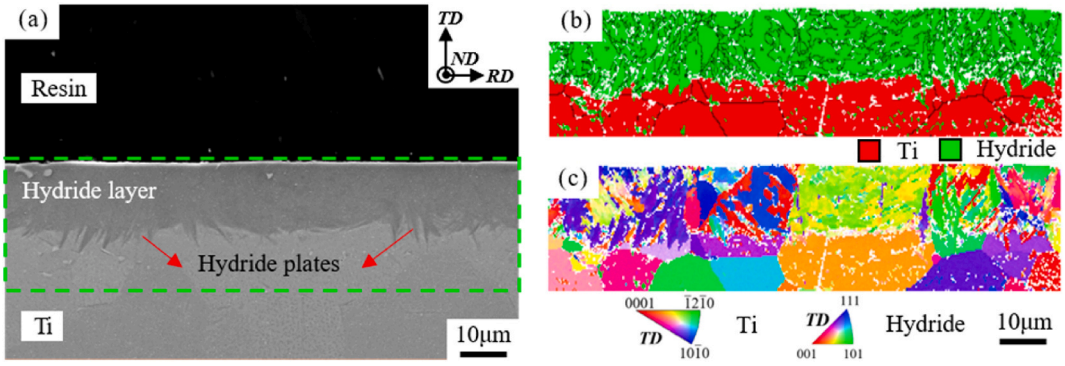

Fig. 2. (a) The SEM image of section microstructure of hydride layer. (b) Phase map of the area inside the green box and (c) corresponding IPF map. The color codes are shown under the maps. Black lines represent the grain boundaries. (For interpretation of the references to color in this figure legend, the reader is referred to the Web version of this article.)

The orientation dependent hydride layer has been investigated in Ref. [14]. The hydride layers in the titanium grains with the orientations of $< 10\bar{1}0 >$ and $< \bar{1}2\bar{1}0 >$ aligned to the diffusion direction mainly encourage OR1 hydrides. The grains with $\{10\bar{1}3\}$ and basal plane parallel to the diffusion surface are favorable for the OR2 hydride layer. However, due to that the interface between hydride layer and titanium matrix was broken by the ion beam polishing, the hydride variants cannot be determined according to the section characterization. In the present work, the SEM image in Fig. 2a reveals the interface traces of some hydride plates at the interface between hydride layer and titanium matrix, which can help identify partial hydride variants.

Fig. 3a shows the magnified SEM image at the interface between hydride layer and matrix. Four hydrides plates inserted into matrix are chosen, of which the interfaces are labeled by the dotted red lines. The

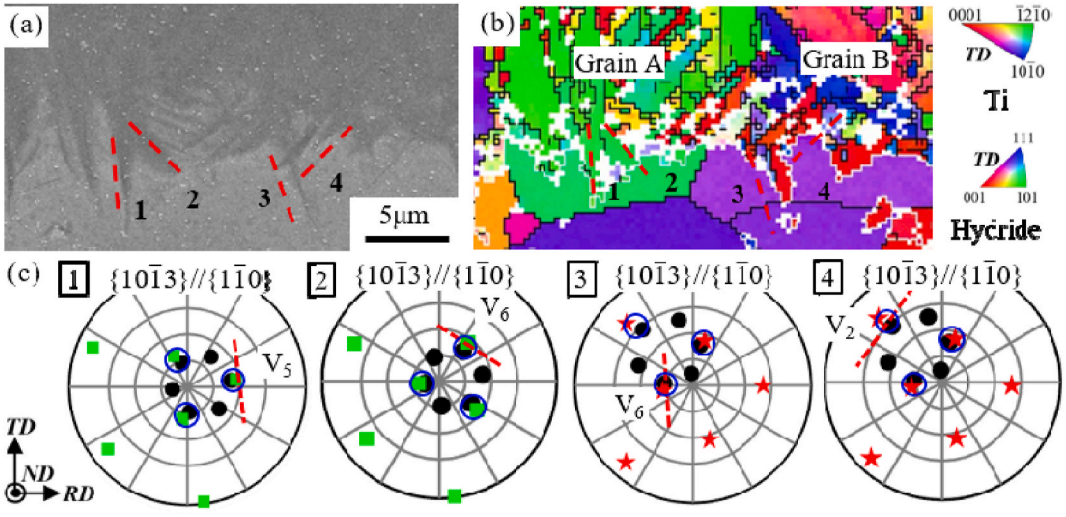

Fig. 3. The magnification images at the interface between Ti matrix and hydride layer, (a) SEM image, (b) IPF map. The grain and phase boundaries are colored by black and white colors, respectively. The dotted red lines show the interface traces of four hydride plates. (c) $\{10\bar{1}\,3\}//\{1\,\bar{1}\,0\}$ plane pole figures of the four hydride variants. The black dots represent the $\{10\bar{1}3\}$ interface planes of Ti grains and the colors represent the $\{1\bar{1}0\}$ interface planes of hydrides. The orientations are Grain A (98.2°, 13.1°, 30.6°), Grain B (35.9°, 142.3°, 18.2°), Hydride 1 (227.1°, 45.0°, 46.2°), Hydride 2 (348.4°, 47.8°, 27.4°), Hydride 3 (77.4°, 16.8°, 15.5°) and Hydride 4 (71.7°, 16.6°, 19.2°). (For interpretation of the references to color in this figure legend, the reader is referred to the Web version of this article.)

corresponding IPF map colored by **TD**//hydrogen diffusion direction is presented in Fig. 3b. The four hydride variants in Fig. 3a belong to two titanium grains (Grain A and Grain B). Based on the orientation relationship in Table 1, all the four hydrides follow OR2. OR2 hydride transformation is achieved by lattice dilatations and a shear of Shockley dislocation, but the shear of OR1 can be self-accommodated [14]. Thus, compared with OR1 hydride, OR2 hydride is more likely to be embedded into titanium matrix to relax the shear deformation during the formation of hydride layer.

The hydride variants of OR2 can be distinguished by their different interface planes $\{10\bar{1}\ 3\}//\{1\ \bar{1}\ 0\}$ in titanium matrix, as shown in Table 2. Six interface planes corresponds to six hydride variants. The pole figures of $\{10\bar{1}\ 3\}//\{1\ \bar{1}\ 0\}$ interface plane of the four hydrides are presented in Fig. 3c. The overlapping poles of $\{10\bar{1}\ 3\}$ and $\{1\bar{1}\ 0\}$ planes inside blue circles mean the possible hydride variants. The unique variant for each hydride can be further determined by the combination of interface trace. Thus, with our method of sample preparation, the variants of part hydrides at the interface between hydride layer and titanium matrix can be identified based on the interface trace in SEM image.

3.1.2. Mechanical properties

The hardness and modulus related to the distance from diffusion surface are presented in Fig. 4a and b, respectively. In Fig. 4a, the indentation hardness slightly increases from 3.3 to 3.5 GPa and suddenly decreases at the distance of 13 μm. Thus, the thickness of hydride layer is around 13 μm with the average hardness 3.4 ± 0.2 GPa. The hardness distribution can be divided into two parts: hydride layer and Ti matrix. The average hardness of titanium matrix is around 3.1 ± 0.4 GPa, lower than hydride layer, which shows the hard nature of titanium hydride. Besides, the hardness of titanium matrix fluctuates more with significant error. Indeed, the hardness of HCP pure titanium is strongly dependent on the crystal orientation [16]. In the five indentation lines across section, the five indents at the same distance from surface can locate in different titanium grains, which leads to the hardness fluctuation. In contrast, the slightly changed hardness inside hydride layer shows less anisotropy of hydride layer.

The distribution of plane strain modulus along hydride layer section is shown in Fig. 4b. The modulus increases rapidly with the increase of distance from surface until 13 μm and then remains almost unchanged in titanium matrix. In contrast with hardness, the stable elastic modulus is less sensitive to orientation in this work. Indeed, the Berkovich tip does not allow to probe the elastic properties of the materials properly, because its salient tip plasticizes rapidly the indented area [25]. The spherical nanoindentation can better measure the anisotropic modulus of titanium [26]. The average modulus of hydride 125.9 ± 8.4 GPa is lower than titanium 138.6 ± 7.4 GPa. Chen et al. [8] proposed that the cracks originate more frequently inside hydride than matrix. The initiated micro-cracks can then result in the reduction of macroscopic elastic modulus [27]. Thus, the hydride layer has lower modulus, that is, lower resistance to elastic (recoverable) deformation under indentation load. In addition, cracks more easily initiate at hydrides in the sample with higher hydrogen content [8]. Thus, the hydride layer closer to the diffusion surface undergoing longer hydrogen charging processing has higher hydrogen content and definitely lower modulus.

3.2. Anisotropic mechanical properties of the diffusion surface

3.2.1. Surface microstructures before and after hydrogen charging

Before studying the anisotropic hardness evolution of Ti surface, the EBSD maps before and after 168 h hydrogenation are performed and shown in Fig. 5. The initial titanium grains are equiaxed and colored by ***ND***//hydrogen diffusion direction in Fig. 5a. After hydrogen charging, a short electropolishing was performed on the diffusion surface to prevent the influence of the corrosion of hydrogen charging solution. The EBSD map is presented in Fig. 5b with hydride phase in ***ND***-IPF color and remnant Ti in black color. In general, more than one hydride variant is formed inside each titanium grain. The different hydride microstructures are dependent on the corresponding grain orientations of titanium matrix [13]. The large distortion of hydride transformation and the variant interactions inside hydride clusters lead to the lower indexation of Fig. 5b.

3.2.2. Anisotropic hardness of α-ti

To calculate anisotropic hardness of α-Ti, 44 α-Ti grains with different orientations are chosen from initial sample to do the indentation test (6 indents for each grain). IPF with average indentation hardness (H_{IT}) scales are drawn in Fig. 6a, which allow the observation of the relationship between the crystallographic orientation of a chosen single grain and corresponding hardness. As shown in Fig. 6a, a clear color gradient appears in the fundamental triangle of IPF showing a significant tendency between the hardness value and specific orientation of individual grain. The hardness value decrease as the ***c***-axis of the HCP crystal deviated from ***ND***. The H_{IT} values of α-Ti are in the range from 3.5 to 2.3 GPa with an average of 2.9 ± 0.4 GPa. The anisotropic hardness of CP-Ti was also measured using indentation (Berkovich tip, maximum load 50 mN) in Ref. [16]. The observed orientation dependence of hardness is consistent with our results.

According to the IPF of hardness in Fig. 6a, there appears the variation of H_{IT} along radial direction but not obvious circumferential variation. Thus, the H_{IT} of CP-Ti is a function of the declination angle (Φ). The declination angle is between *c*-axis of the HCP crystal and the normal of sample surface (***ND***), which is equal to the second angle Φ of Euler angle (φ1, Φ, φ2). The only radial variation of hardness shows negligible influence of (φ1, φ2). Indeed, the result of crystal elastic finite element simulation on hardness of CP-Ti proposed negligible influence of (φ1, φ2) [26]. Fig. 6b shows the relationship between indentation hardness and declination angle (Φ). In general, the H_{IT} values monotonously decrease from 3.5 to 2.3 GPa as the indentation direction (stress axis) deviates from *c*-axis. It marginally decreases 3.4% at $0^\circ < \Phi < 30^\circ$ and 7.2% at $70^\circ < \Phi < 90^\circ$, decreases steeply by approximately 22.6% within $30^\circ < \Phi < 70^\circ$. These trends demonstrate strong dependence between indentation hardness of individual grain and the orientation of indentation direction. The *c*-axis parallel to stress axis ($\Phi = 0^\circ$) is the hardest orientation, while the $< 10\bar{1}0 >$ or $< 1\bar{2}10 >$ along stress axis ($\Phi = 90^\circ$) is softest orientation for indentation test.

Indentation hardness measures the resistance of CP-Ti to local plastic deformation produced by compression load from an indenter, thus the orientation dependent H_{IT} is attributed to the anisotropic activation of slip and twinning systems. The stress to activate a given slip or twinning system is proportional to CRSS/SF (CRSS: critical resolved shear stress, SF: Schmid factor). Viswanathan et al. [28] characterized plastic zone of α-Ti beneath nanoindents with focused-ion-beam (FIB) and transmission electron microscopy (TEM) techniques. $<c+a>$ slip is most favorable system in the hardest grain, all three types of $<a>$ slips (prismatic, basal

Table 2
The interface planes of hydride variants.

Variant	Variant 1	Variant 2	Variant 3	Variant 4	Variant 5	Variant 6
Interface	$(10\bar{1}3)//(1\bar{1}0)$	$(01\bar{1}3)//(1\bar{1}0)$	$(\bar{1}103)//(1\bar{1}0)$	$(\bar{1}013)//(1\bar{1}0)$	$(0\bar{1}13)//(1\bar{1}0)$	$(1\bar{1}03)//(1\bar{1}0)$

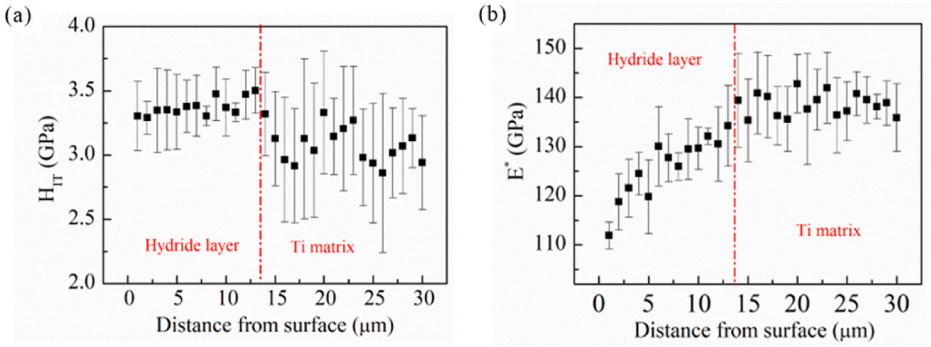

Fig. 4. The distributions of (a) indentation hardness and (b) modulus versus distance from surface on the hydrogen diffusion section. Error bars are ± one standard deviation which incorporates five measurements in the same distance.

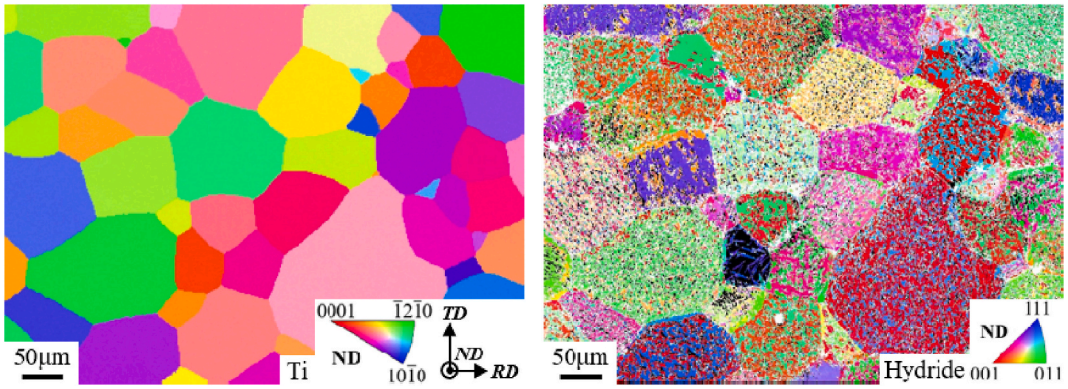

Fig. 5. (a) ***ND***-IPF map of α-Ti before charging. (b) EBSD map of hydride layer after charging. Hydride phase is IPF-colored and Ti phase in black color. (For interpretation of the references to color in this figure legend, the reader is referred to the Web version of this article.)

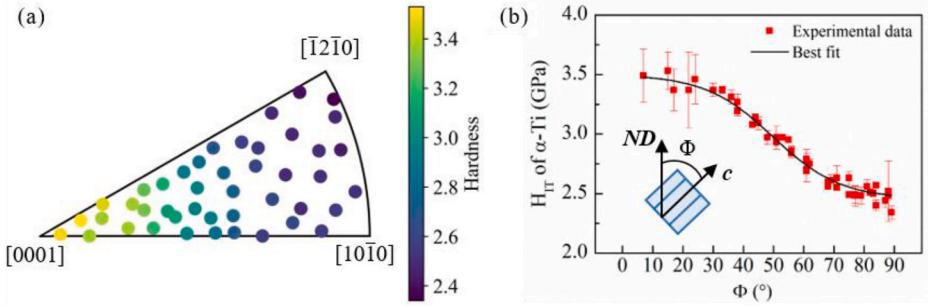

Fig. 6. (a) Indentation hardness IPF of α-Ti before charging. (b) Indentation hardness versus declination angle (Φ). Error bars are ± one standard deviation which incorporates multiple measurements in the same grain.

and pyramidal) are activated in the medium grain and screw prismatic <*a*> slip is predominant in softest grain. For CP-Ti, the CRSS for activation of <*c*+*a*> and prismatic <*a*> dislocations at room temperature are around 141 and 350 MPa, respectively [29]. It means that, if the SFs of <*c*+*a*> and prismatic <*a*> dislocation are the same, the stress needed for <*c*+*a*> dislocation is 2.5 times larger than that of prismatic <*a*>. Thus, the difference on activation stresses of multiple slip systems is the main reason for the anisotropic hardness. Twinning was not observed whether outside or beneath the residual indent [26,28]. Because of significant size dependence, large indenter size is needed to activate deformation twinning [30].

SF is calculated to evaluate the probability of slip activation in the grain with different orientation under indentation compression. The grains with Euler angles of [0°, 0°, 0°] and [0°, 0°, 15°] are taken as two initial orientations, which are the hardest orientations with *c*-axes parallel to stress direction, and then misoriented through alter the angle Φ from 0° to 90°. For each orientation, the maximum SFs among the variants in each slip system are calculated and shown in Fig. 7. The lines with different colors represent five slip systems in CP-Ti. The solid and dotted lines show the SFs of the grain oriented from respective [0°, 0°, 0°] and [0°, 0°, 15°]. At Φ = 0°, all the SFs of <*a*> slips are almost zero, the activation of them is severely limited, thus <*c*+*a*> slips with large SF (>0.4) are favorable in this orientation leading to the larger hardness. As the angle Φ increases, the orientation gradually favors <*a*> slips and the hardness decreases. In the medium grain (Φ = 45°), the SF of basal slip is highest, while the other <*a*> slips with slightly lower SF can also be activated due to the lower CRSS. The softest orientation of Φ = 90° has the highest SFs for prismatic slip, which is the most common slip system in CP-Ti. Therefore, in this orientation, plastic deformation can be easily stimulated with low applied stress of indentation test.

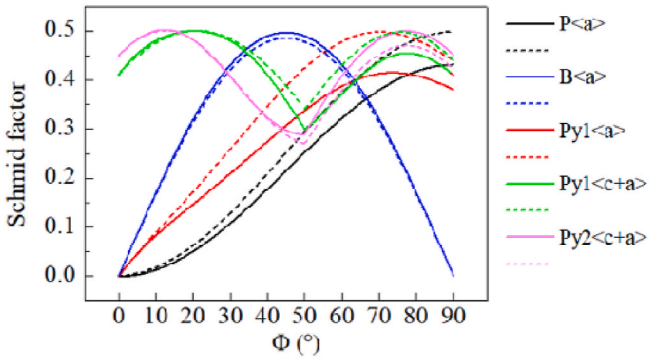

Fig. 7. Schmid factor value of the dislocation slip systems with angle between the *c*-axis and loading direction.

3.2.3. *Anisotropic hardness of δ-hydride*

After hydrogen charging, indentation tests were performed on the same 44 grains in order to compare the hardness change. The hardness IPF of the hydride corresponding to titanium grain orientations is drawn in Fig. 8a. The H_{IT} values of hydride are in the range from 4.2 to 2.5 GPa with an average of 3.3 ± 0.4 GPa, which is around +13.8% larger than α-Ti matrix (2.9 ± 0.4 GPa). The hardness of hydride layer shows less sensitive orientation dependence. The slightly higher hardness (inside red circle) always occurs in the titanium grain with $\{10\bar{1}3\}$ nearly parallel to ***ND*** surface, which is the most favorable orientation for OR2 hydride. The summary of H_{IT} versus declination angle Φ is shown in Fig. 8b. There appears a peak at around Φ = 30° corresponding to the orientation with higher hardness in Fig. 8a. The distribution of hydride hardness shows more scattered with greater error, which will be further studied in Section 3.2.4.

3.2.4. *Hardness change before and after hydrogen charging*

To study the hardness change, the indentation hardness of 44 selected grains before and after charging is present in the same graph (Fig. 9) versus the ***c***-axis declination angle Φ. The hardness of titanium matrix decreases with the increase of angle Φ, while the hardness values of hydrides are always higher than titanium. Interestingly, the hardness distribution of hydrogenated surface is also related to the orientation of titanium matrix, which can be divided into four parts. In Part 1 and Part 3, the hardness of hydride is close to titanium, but the hydride hardness is much higher than titanium in Part 2 and Part 4. The hardness fluctuation of hydrogenated surface can be due to the variety of hydride microstructure.

The hydride cluster microstructure (SEM image and corresponding EBSD maps) of four grains respectively in the four parts are shown in Fig. 10. In the EBSD maps, the hydride is in ***ND***-IPF color and titanium phase is black. The hydride fractions in Grain 2 and Grain 4 are much higher than Grain 1 and Grain 3. The orientations of Grain 2 and Grain 4 close to the most favorable ones for hydride transformation: $\{10\bar{1}3\}$ or

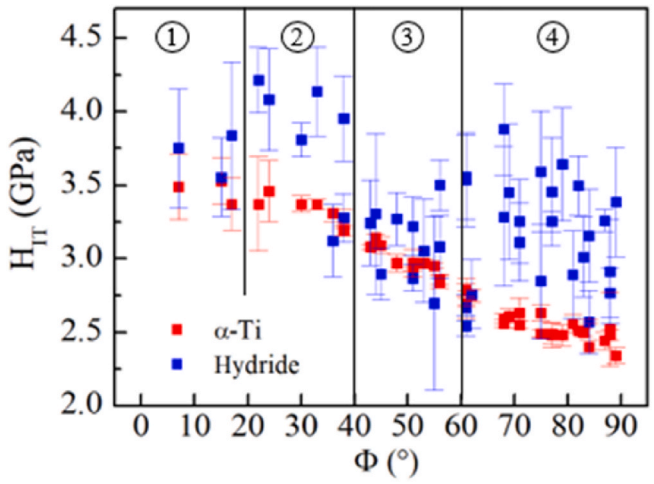

Fig. 9. The change of H_{IT} on sample surface before and after hydrogenation. Error bars are ± one standard deviation which incorporates multiple measurements in the same grain.

$\{10\bar{1}0\}$ interface planes parallel to the diffusion surface [13]. Therefore, the grain with favorable orientation can form denser hydride layer.

It can be derived that the hardness fluctuation of hydrogenated surface in Fig. 9 is mainly due to the different fractions of hydride phase in hydride layer. The six 2 × 3 indentations and one ADO can be found in SEM images and are non-indexed in EBSD maps. In Grain 1 and Grain 3, due to the lower hydride fraction, some indentations are pressed in titanium matrix or at hydride-matrix interface, which reduces the average hardness of the hydrogenated grains. As for Grain 2 and Grain 4, the denser hydride layer significantly increase the hardness of diffusion surface. Besides, the hardness error of hydrogenated surface is larger due to the complicated interaction between hydride cluster and titanium matrix. The indentations pressed into hydride-hydride interface, hydride-matrix interface or titanium matrix increase the standard deviation.

4. Conclusion

The microstructure and mechanical properties of hydrogen diffusion section and surface were investigated in the present work. The following conclusions can be drawn:

(1) The clear section microstructure of hydride diffusion layer is observed for the first time and shows the non-uniform hydride formation during the hydrogen charging at room temperature. Partial hydride variants near the interface between hydride layer and titanium matrix can be determined based on the trace direction of hydride plates.

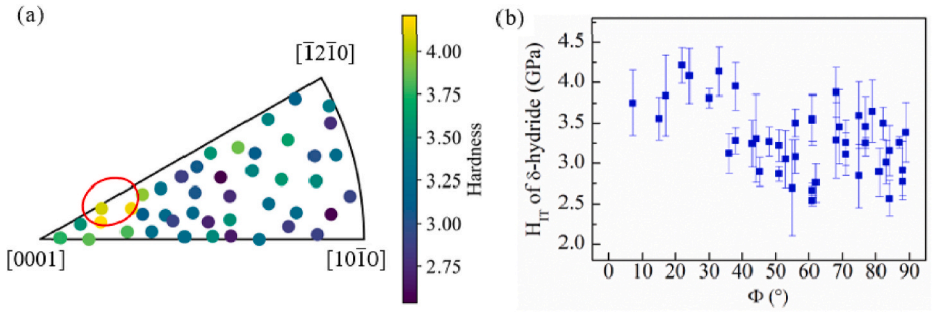

Fig. 8. (a) Hardness IPF of hydride drawn with orientation of Ti matrix. (b) Indentation hardness of δ-hydride layer versus declination angle Φ. Error bars are ± one standard deviation which incorporates multiple measurements in the same grain.

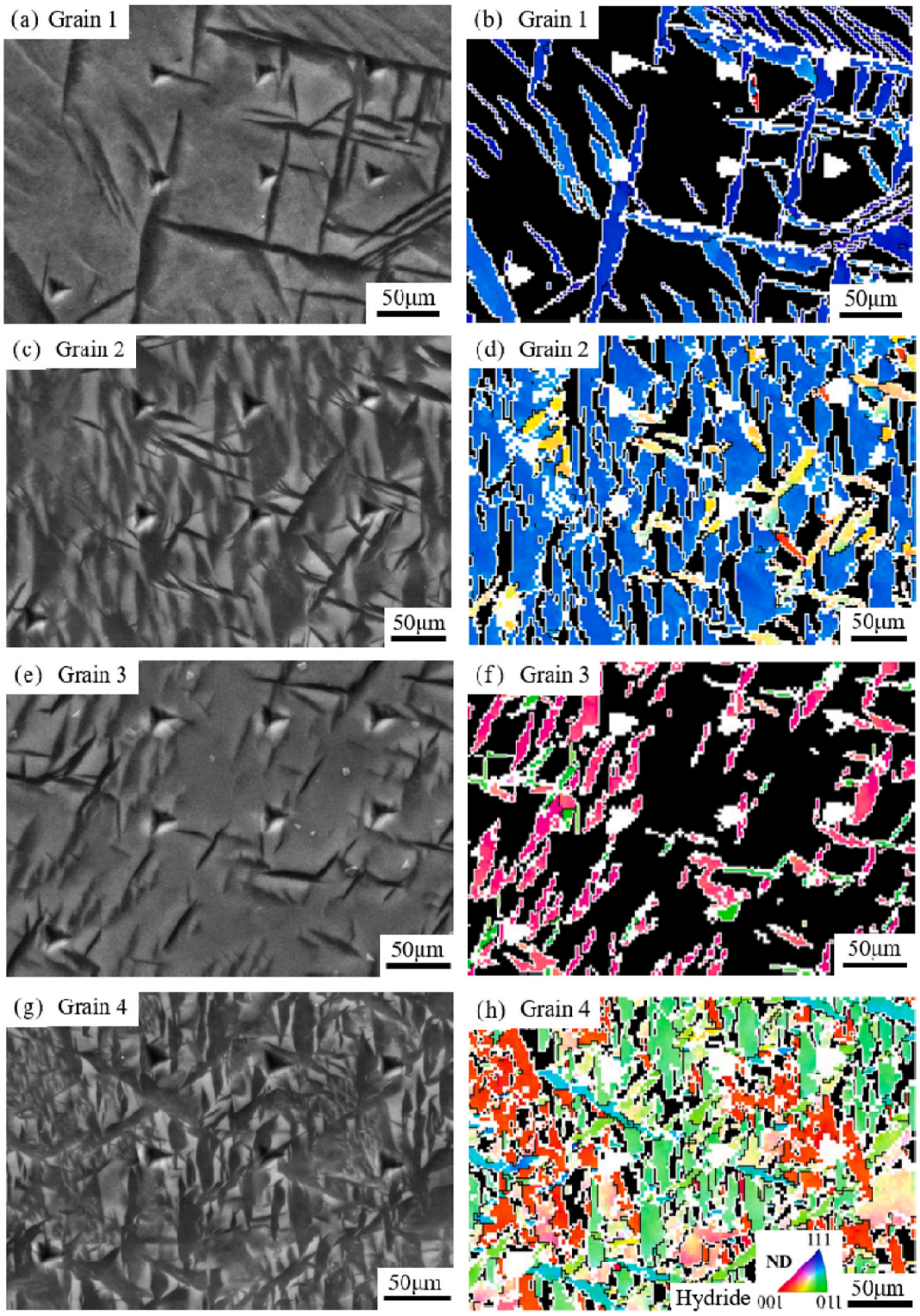

Fig. 10. SEM images and corresponding EBSD maps in the indentation areas of four grains. (a) and (b) are Grain 1 in Part 1, (c) and (d) are Grain 2 in Part 2, (e) and (f) are Grain 3 in Part 3, (g) and (h) are Grain 4 in Part 4. In the EBSD maps, hydride is IPF-colored and titanium in black color. The grain and phase boundaries are colored by black and white colors, respectively. (For interpretation of the references to color in this figure legend, the reader is referred to the Web version of this article.)

(2) According to the indentation tests across the hydride layer, the hard nature of hydride leads to the higher hardness of hydride layer than titanium matrix. There appears more considerable anisotropy of hardness in titanium than hydride layer. The modulus increases rapidly with the increase of distance from diffusion surface and is almost unchanged in titanium matrix.

(3) The anisotropic hardness of diffusion surface is studied before and after hydrogen charging. The hardness of titanium matrix decreases with the increase of deviation angle between ***c***-axis and

surface normal. In the titanium grain with more favorable orientation for hydride transformation, the formed hydride layer tends to be denser and possess higher indentation hardness.

CRediT

Qian Wang:Methodology, Investigation, Writing - original draft, Validation. **Jean-Sébastien Lecomte**: Conceptualization, Methodology, Supervision, Writing - review & editing. **Christophe Schuman**: Conceptualization, Methodology, Supervision, Writing - review & editing. **Laurent Peltier**: Methodology, Investigation.

Declaration of competing interest

The authors declare that they have no known competing financial interests or personal relationships that could have appeared to influence the work reported in this paper.

Acknowledgements

The authors would like to thank Prof. Eric Fleury for the loan of the hydrogen charging device. The first author Qian Wang is grateful to the China Scholarship Council for the support of her PhD study in France.

References

[1] M.H.O. Könönen, E.T. Lavonius, J.K. Kivilahti, SEM observations on stress corrosion cracking of commercially pure titanium in a topical fluoride solution, Dent. Mater. 11 (1995) 269–272.
[2] D.S. Shih, I.M. Robertson, H.K. Birnbaum, Hydrogen embrittlement of alpha titanium : in situ TEM studies, Acta Metall. 36 (1988) 111–124.
[3] E. Conforto, D. Caillard, A fast method for determining favourable orientation relationships and interface planes: application to titanium-titanium hydrides transformations, Acta Mater. 55 (2007) 785–798.
[4] A. Bourret, A. Lasalmonie, S. Naka, In-situ high resolution observation of hydride precipitation in titanium, Scripta Metall. 20 (1986) 861–866.
[5] H. Numakura, M. Koiwa, Hydride precipitation in titanium, Acta Metall. 32 (1984) 1799–1807.
[6] E. Conforto, D. Caillard, Edge-to-edge matching at Ti-TiH interfaces: kinetics of hydride growth and clustering of precipitates with different orientation relationships, Solid State Phenom. 172–174 (2011) 242–247.
[7] O.T. Woo, G.C. Weatherly, C.E. Coleman, R.W. Gilbert, The precipitation of γ-deuterides (hydrides) in titanium, Acta Metall. 33 (1985) 1897–1906.
[8] C.Q. Chen, S.X. Li, H. Zheng, L.B. Wang, K. Lu, An investigation on structure, deformation and fracture of hydrides in titanium with a large range of hydrogen contents, Acta Mater. 52 (2004) 3697–3706.
[9] J.J. Xu, H.Y. Cheung, S.Q. Shi, Mechanical properties of titanium hydride, J. Alloys Compd. 436 (2007) 82–85.
[10] Q. Wang, J.-S. Lecomte, C. Schuman, A. Mandrelli, The mechanical property evolution and grain boundary accommodation during hydride transformation in commercial pure titanium, Mater. Sci. Eng. A. 812 (2021) 141099.
[11] E. Conforto, B.-O. Aronsson, A. Salito, C. Crestou, D. Caillard, Rough surfaces of titanium and titanium alloys for implants and prostheses, Mater. Sci. Eng. C 24 (2004) 611–618.
[12] E. Conforto, D. Caillard, B.-O. Aronsson, P. Descouts, Crystallographic properties and mechanical behaviour of titanium hydride layers grown on titanium implants, Philos. Mag. A 84 (2004) 631–645.
[13] Q. Wang, S. Xu, J.S. Lecomte, C. Schuman, L. Peltier, X. Shen, W. Song, Crystallographic orientation dependence of hydride precipitation in commercial pure titanium, Acta Mater. 183 (2020) 329–339.
[14] Q. Wang, S. Xu, Y. Zhao, J.-S. Lecomte, C. Schuman, Multi-dimensional morphology of hydride diffusion layer and associated sequential twinning in commercial pure titanium, J. Mater. Sci. Technol. 103 (2022) 105–112.
[15] K. Tougou, T. Onitsuka, K. Fukumoto, M. Uno, H. Muta, The study of hardening evaluation of pure Zr with δ-hydrides generation by the dynamic in-situ metallic structure observation and nano-indentation hardness test, J. Nucl. Mater. 511 (2018) 284–296.
[16] C. Fizanne-Michel, M. Cornen, P. Castany, I. Péron, T. Gloriant, Determination of hardness and elastic modulus inverse pole figures of a polycrystalline commercially pure titanium by coupling nanoindentation and EBSD techniques, Mater. Sci. Eng. A. 613 (2014) 159–162.
[17] A. Fitzner, J. Palmer, B. Gardner, M. Thomas, M. Preuss, J.Q. da Fonseca, On the work hardening of titanium: new insights from nanoindentation, J. Mater. Sci. 54 (2019) 7961–7974.
[18] F. Qiang, E. Bouzy, H. Kou, Y. Zhang, L. Wang, J. Li, Grain fragmentation associated continuous dynamic recrystallization (CDRX) of hexagonal structure during uniaxial isothermal compression: high-temperature α phase in TiAl alloys, Intermetallics 129 (2021) 107028.
[19] G. Vander Voort, Metallographic preparation of titanium and its alloys, Buehler Tech-Notes. 3 (1999).
[20] J. Wen, N. Allain, E. Fleury, Determination of orientation relationships between FCC-hydride and HCP-titanium and their correlation with hydrides distribution, J. Alloys Compd. 817 (2020) 153297.
[21] W.C. Oliver, G.M. Pharr, Measurement of hardness and elastic modulus by instrumented indentation: advances in understanding and refinements to methodology, J. Mater. Res. 19 (2004) 3–20.
[22] H. Somekawa, T. Mukai, Nanoindentation creep behavior of grain boundary in pure magnesium, Phil. Mag. Lett. 90 (2010) 883–890.
[23] J. Wen, N. Main, E. Fleury, The effect of hydrogen-deformation interactions on recrystallization of β-21S titanium alloys, Proc. 13th World Conf. Titan. (2016) 275–280.
[24] M.A. Rodríguez, Anticipated degradation modes of metallic engineered barriers for high-level nuclear waste repositories, JOM 66 (2014) 503–525.
[25] R.A. Mirshams, R.M. Pothapragada, Correlation of nanoindentation measurements of nickel made using geometrically different indenter tips, Acta Mater. 54 (2006) 1123–1134.
[26] J.S. Weaver, M.W. Priddy, D.L. McDowell, S.R. Kalidindi, On capturing the grain-scale elastic and plastic anisotropy of alpha-Ti with spherical nanoindentation and electron back-scattered diffraction, Acta Mater. 117 (2016) 23–34.
[27] F.C.S. Carvalho, J.F. Labuz, Experiments on effective elastic modulus of two-dimensional solids with cracks and holes, Int. J. Solid Struct. 33 (1996) 4119–4130.
[28] G.B. Viswanathan, E. Lee, D.M. Maher, S. Banerjee, H.L. Fraser, Direct observations and analyses of dislocation substructures in the α phase of an α/β Ti-alloy formed by nanoindentation, Acta Mater. 53 (2005) 5101–5115.
[29] K.E.K. Amouzou, T. Richeton, A. Roth, M.A. Lebyodkin, T.A. Lebedkina, Micromechanical modeling of hardening mechanisms in commercially pure α-titanium in tensile condition, Int. J. Plast. 80 (2016) 222–240.
[30] S. Pathak, S.R. Kalidindi, N.A. Mara, Investigations of orientation and length scale effects on micromechanical responses in polycrystalline zirconium using spherical nanoindentation, Scripta Mater. 113 (2016) 241–245.